A First-Principles Study of Multilayer Ti₃C₂T_x MXene Model

Model Yi Zhi Chu^{1,2}, Kah Chun Lau^{2*} ¹Department of Physics, Michigan Technological University, Houghton, MI 49931, USA ²Department of Physics and Astronomy, California State University, Northridge, CA 91330, USA *Correspondence: kahchun.lau@csun.edu

ABSTRACT

We propose a more realistic albeit slightly complicated multilayer Ti₃C₂T_x model and performed a comprehensive theoretical study of the structural and electronic properties. In this work, we constructed various multilayer Ti₃C₂T_x structures considering different concentrations of hydrofluoric acid, HF (5, 10, and 48 wt. %) as the etchant. The validity of our ternary mixed O/OH/F-terminated Ti₃C₂T_x multilayer models is confirmed with the consistency of the calculated d-spacing (9.60 \pm 0.07 Å), simulated X-ray diffraction (XRD) spectra and the predicted adhesion energy $(0.77 \pm 0.15 \text{ J/m}^2)$ with the reported experimental measurements. The uniform terminated and mixed terminated multilayer Ti₃C₂T_x exhibit metallic characteristics, similar to those of monolayer $Ti_3C_2T_x$. We found a stronger interaction between the interlayers with OH-rich ternary mixed terminated Ti₃C₂T_x surfaces, due to the formation of hydrogen bonds between the hydroxyl groups and adjacent layers of F/O terminal groups as supported by the crystal orbital Hamilton population (COHP) calculation. From this finding, we propose that multilayer $Ti_3C_2T_x$ etched with a strong HF acid could be easier to exfoliate into monolayer sheets due to smaller adhesion energy. Based on this work, we believe that current findings will offer a fundamental understanding and a useful baseline multilayer model for the future investigation of the hydrogen and ions storage and diffusion capabilities in the MXene multilayer application.

1. INTRODUCTION

MXenes have rapidly grown into the largest two-dimensional (2D) material family since the successful experimental synthesis of its pioneering material, Ti₃C₂T_x in 2011 ^{1, 2}. For Ti₃C₂T_x, T_x is the surface terminal group comprised of O, OH, F, or Cl depending on the experimental used etchant. Due to their 2D morphology, metallicity, and high tunability of surface termination, they exhibit promising potential applications in a vast realm, such as gas sensors ³ and energy storage ⁴⁻⁷. One of the studies that has recently garnered significant interest is its capability for hydrogen storage ⁶⁻¹⁰. Recently, using mixed terminated surfaces, we investigated the hydrogen storage capabilities of the Ti₃C₂T_x monolayers and found that mixed terminated surfaces demonstrated unique electronic properties that were otherwise absent on the uniformly F/O/OH-terminated surfaces, which are beneficial for hydrogen adsorption⁷. The theoretical study reveals the tunability of hydrogen adsorption energy with different surface terminal group. However, the surface hydrogen adsorption study only accounts for the storage capacity utilizing the basal plane of the

 $Ti_3C_2T_x$ surface considering the effect of surface termination, while the important interlayer adsorption that offers another hydrogen storage avenue was not readily considered.

1

2

3

4

5

6

7

8

9

10

11

12

13

14

15

16

17

18

19

20

21

22

23

24

25

26

27

28

29

30

31

In a recent review article on the MXene as hydrogen storage material, Thomas et al. 10 conducted a thorough literature search on the hydrogen storage performance of a variety of MXenes and concluded that there remain plenty of challenges that needed to be addressed for MXenes to be considered a viable candidate for hydrogen storage. Among the unanswered questions was, how would the hydrogen molecules diffuse and store in the multilayer Mxene. Early theoretical hydrogen storage study of graphene nanostructure by Patchkovskii ¹¹ demonstrated that the enhanced hydrogen storage capacity attributed to the "nano pump" effect, where the hydrogen pressure in the small gap between the interlayer structure is increased due to the confinement of hydrogen molecules at interlayers. A more recent study of the hydrogen storage in graphene-based sandwich structures¹² also showed a tunable hydrogen storage capacity by increasing the amount of hydrogen molecules capsuled inside the interlayer. On the other hand, for MXenes, one of their advantages is their 2D morphology and adjustable interlayer spacing that is useful for controlling the diffusion and adsorption of hydrogen gas, and potentially enhancing the overall storage capacity of hydrogen. To date, two experimental measurements of the hydrogen storage capacity of Ti-based MXenes have been reported. Liu et al. 8 studied the correlation between the interlayer spacing and hydrogen storage capacity of incompletely etched MXenes (Ti₃C₂T_x and Ti₂CT_x) and suggested that the hydrogen storage in the interlayer is possibly due to the nano pump-assisted weakly chemical absorption of hydrogen. Ghotia et al. 9 et al also observed a high storage capacity of Ti₃C₂T_x at cryogenic temperature and 2.5 MPa of hydrogen pressure. However, the fundamental understanding of the storage mechanism remains elusive despite these experimental reports. Nevertheless, these studies have suggested that the interlayer of MXenes possibly plays a pivotal role in optimizing the hydrogen storage capacity in Ti₃C₂T_x MXenes. Therefore, it is paramount to understand the structural properties of and the interaction between the multilayer $Ti_3C_2T_x$ to reveal its hydrogen storage mechanism and the full hydrogen storage capability.

The first $Ti_3C_2T_x$ was exfoliated from the Ti_3AlC_2 using 50 wt. % HF ¹. Ying et al. ¹³ first synthesized the $Ti_3C_2T_x$ using 10 wt. % HF and observed a relatively large d-spacing of ~13.5 Å. In a later study by Wang et al. ¹⁴, they observed a significant drop in the d-spacing upon drying of the sample after washing, thus, hypothesizing such large d-spacing as observed in the study of Ying et al. ¹³ could be attributed to the presence of water or aqueous solution in between the MXene

layers. In a recent work, Wang et al. ¹⁵ studied the effect of HF etching time on the MXene structure and found a variation of *d*-spacing from 9.3 to 9.87 Å after 17 days of etching. Other experimental syntheses of Ti₃C₂T_x with different HF concentrations (5-50 wt. %) demonstrated that the *d*-spacing of synthesized multilayer Ti₃C₂T_x is in the range of 9.5 to 9.9 Å ^{16, 17}. However, despite more than a decade of discovery, the characterization of the surface distribution of the terminating group on Ti₃C₂T_x remains a challenging task as it is hindered by the insensitivity to hydrogen employing those methods ^{1, 17}. Nevertheless, the fundamental understanding of the surface morphology and subtle interlayer interaction within the multilayer Ti₃C₂T_x remains lacking. A thorough and systematic study of multilayer Ti₃C₂T_x with ternary mixed F/O/OH-termination remains absent from the literature. A systematic basic study thus is crucial for providing a design principle for these structural properties, and hydrogen storage application. To fill this literature gap, we intend to carry out a baseline study exploring the structural and electronic properties of multilayer ternary mixed F/O/OH-terminated multilayer Ti₃C₂T_x multilayers, in comparison to the surface adsorption of hydrogen on the mixed F/O/OH Ti₃C₂T_x monolayers⁷.

1 2

Meanwhile, recent experimental efforts have been carried out to understand the surface terminal group distribution on Ti₃C₂T_x. For instance, using pair distribution function (PDF) in the energy-dispersive X-ray spectroscopy (EDX) characterization, Wang et al. 14 determined the stoichiometry of T_x based on the average atomic ratio of O:F in the multilayer $Ti_3C_2T_x$ sample. Based on this reported experimental study, we have investigated the structural and electronic properties of Ti₃C₂T_x monolayers¹⁸, going beyond the first- and second-generation models of MXenes monolayers which consider either a bare or uniformly terminated $Ti_3C_2T_x$ with a single terminating functional group^{14, 18}. Recently, Marquis et al. ¹⁹ studied the binary/ternary mixed terminated multilayer Ti_2CT_x ($T_x = O, F, OH$) structures and found that surface termination plays an important role in tuning the MXenes tribological properties in experiments. This implies that surface termination indeed affects the interlayer interaction and potentially the hydrogen diffusion and storage in the multilayer MXenes. To go beyond the monolayers study^{7, 18} and to extend the current limited understanding in multilayer Ti₃C₂T_x model, in this work, considering various $Ti_3C_2T_x$ surfaces, i.e., the uniformly terminated $Ti_3C_2T_x$ surfaces ($T_x = F_2$, O_2 or OH_2) and the ternary mixed terminated surfaces $Ti_3C_2T_x(T_x = O_pOH_qF_r)$, where p + q + r = 2 adopted from Ref¹⁸, we have constructed various multilayer $T_{i_3}C_2T_x$ structures representing different etching conditions

(5, 10, 48 wt. % HF) for a systematic structural and electronic properties study based on first-principles calculations.

3

1

2

2. COMPUTATIONAL METHODS AND DETAILS

5 6 7

8

9

10

1112

13

14

15

16

17

18

19

20

21

22

23

24

25

26

To model the multilayer $Ti_3C_2T_x$ structures, first-principles density functional theory (DFT) was employed as implemented in Vienna Ab initio Simulation Package (VASP) ^{20, 21}. The projector-augmented-wave (PAW) pseudopotential method, together with the generalized gradient approximation (GGA) and the Perdew-Burke-Ernzerhof (PBE) exchange-correlation functional were used to represent the exchange-correlation effects in the DFT simulation ²². The kinetic energy cutoff for the plane-wave basis was set at 500 eV. For the structural optimization, the Brillouin zone was sampled using a single k-point, while electronic calculations employed a Γcentered grid of $(3 \times 3 \times 3)$. The electronic self-consistent cycle energy convergence was set at $1 \times 10^{-5} eV$ and the residual force on each atom is less than $1 \times 10^{-4} eV/\dot{A}$. The van der Waals interaction was included in all calculations using the semi-empirical approach of Grimme (DFT-D3) 23 as its reliability has been demonstrated in the previous studies of stacked $Ti_3C_2T_x$ bilayer 24 -²⁶. To investigate the bonding strength between the interlayer structures, crystal orbital Hamilton population (COHP) analysis was carried out as implemented in the LOBSTER code ²⁷⁻³⁰ employing the Bunge basis sets 31 . To further confirm the thermal stability of these multilayer $Ti_3C_2T_x$ at room temperature, ab initio molecular dynamics (AIMD) was performed on one of the structures for 5 ps in the NVT ensemble employing Nosé –Hoover thermostats, and the result is shown in Figure S1. Our calculation shows no significant structure deformation or dissociation of termination groups upon heating at T = 300 K, confirming the thermal stability of our optimized structures at room temperature. All atomic structures and charge densities are visualized using the open-sourced visualization software VESTA 32.

27

3. RESULTS AND DISCUSSIONS

28 29 30

3.1 Model construction

31 32

33

To model multilayer $Ti_3C_2T_x$, we considered the uniform O/OH/F-terminated and the O/OH/F ternary mixed terminated monolayers as adopted from Ref¹⁸ that are found to be

1 thermodynamically stable and more favorable than uniform O/OH/F-termination. To investigate 2 the favorable stacking orientation, the uniform O/OH/F-terminated monolayers were stacked 3 parallelly in the lateral c direction with two different lateral positions (Figure 1), namely the P-4 trigonal and P-octahedral as distinguished by the coordination of the interlayer terminating groups. 5 The "P" denotes the parallel orientation of the monolayers in between the bulk multilayer as shown 6 in Figure 1. For P-trigonal stacking, the adjacent terminating groups face each other directly while 7 the terminating groups in P-octahedral staking face the adjacent outermost Ti atoms. Interestingly, 8 upon full geometrical optimization, we found that the total energy of the P-octahedral stacking is 9 always energetically more favorable than that of the P-trigonal stacking regardless of the 10 terminating group (Table S1). Moreover, for uniform O-terminated monolayer, even starting with 11 the initial stacking of P-trigonal, full geometrical optimization eventually leads to the P-octahedral 12 stacking. To further inspect the relative stability of the P-octahedral and P-trigonal stacked 13 multilayers with comparable d-spacing, we modified the P-trigonal stacked uniform terminated 14 $T_{i_3}C_2T_x$ and two mixed terminated $T_{i_3}C_2T_x$ ($T_x = O_{0.24}OH_{1.28}F_{0.48} & O_{0.24}OH_{0.64}F_{1.12}$) such that their 15 d-spacings are comparable to that of the more stable P-octahedral stacked multilayers or 16 experimental values and performed atomic optimization with the fixed d-spacing. Notably, all the 17 total energies of the P-trigonal stacked multilayers with modified d-spacing, including the mixed 18 terminated Ti₃C₂T_x are found less stable compared to the P-octahedral. For all mixed terminated 19 Ti₃C₂T_x multilayers, we observed that all the optimized structures exhibited stacking order 20 resembling the P-octahedral stacking (Figure S2), and is stable at room temperature according to 21 AIMD simulation (Figure S1). Thus, the P-octahedral stacking is found to be more favorable 22 compared to that of P-trigonal. Further structural properties such as the d-spacing will be discussed 23 in the following Section 3.2.

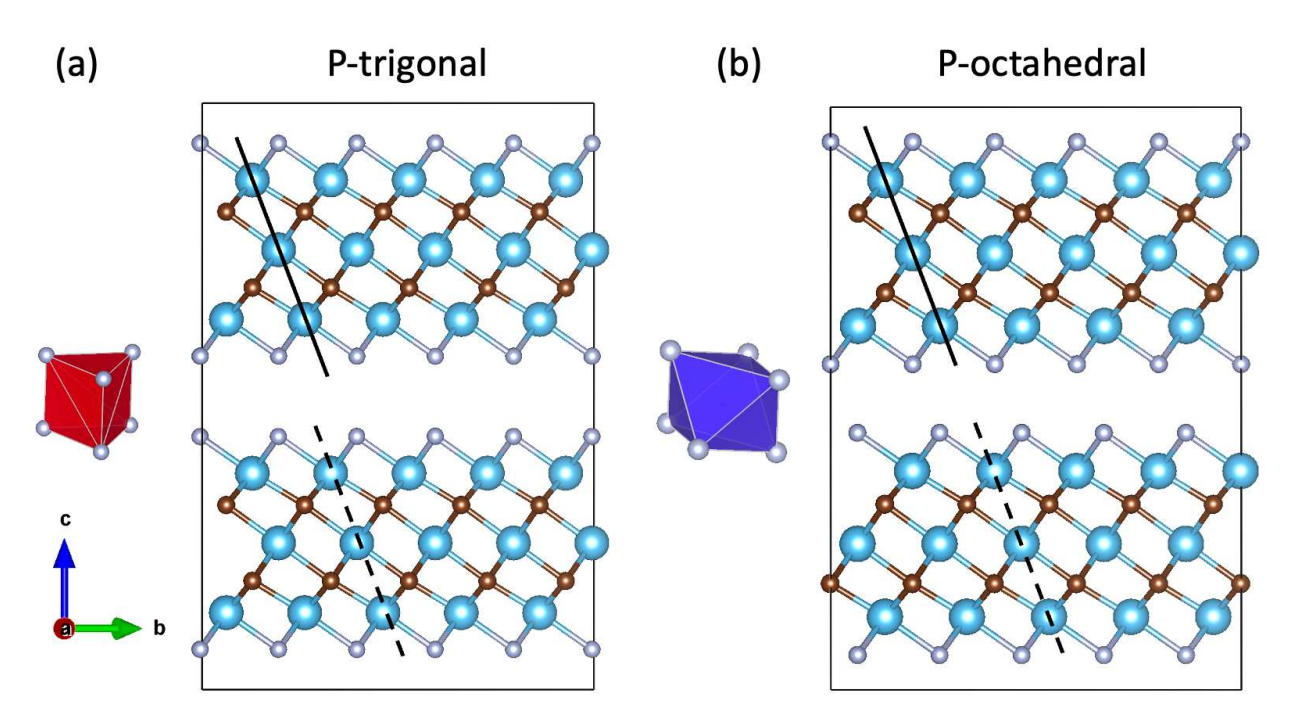


Figure 1. Multilayer $Ti_3C_2T_x$ with (a) P-trigonal and (b) P-octahedral stacking. The terminating groups in (a) are facing directly toward the adjacent layer of terminating groups while terminating groups in (b) are facing toward the adjacent layer of outermost Ti atoms. The P-trigonal stacking in (a) results in the adjacent terminating groups forming a trigonal coordination while P-octahedral stacking in (b) results in an octahedral coordination. The black solid and dotted lines demonstrate the parallel orientation and the relative position of the monolayers in the multilayer structure. Color code- Blue-Ti, Brown-C, Grey-O/OH/F.

3.2 Structural properties of multilayer $Ti_3C_2T_x$

1 2

Figure 2(a) shows the side view of the ternary mixed O-/OH-/F-terminated multilayer bulk structure of $Ti_3C_2T_x$. The d-spacing is defined as the distance between the two adjacent layers of middle Ti atoms [Ref??]. Figure 2(b) shows the simulated X-ray diffraction (XRD) of the ternary mixed terminated $Ti_3C_2T_x$ with different stoichiometry, etched with 5 and 48 wt.% HF. Notably, the signature peak of XRD, *i.e.*, the (002) plane is found in the range of 9.15-9.38° and the location of the (00l) peaks is distinctly recognizable at the respective angles, which is consistent with the experimental observations $^{14, 15, 17, 33}$. In addition, the calculated average d-spacing is 9.60 \pm 0.07 Å, close to the reported d-spacing from experiments (~9.5-9.9 Å). For the multilayer structures with uniform termination, the relative intensity of the (002) peak of $Ti_3C_2O_2$ (Figure S3) is found

to be smaller compared to the (006) peak. In addition, the calculated *d*-spacing for Ti₃C₂O₂ and Ti₃C₂F₂ are 9.2 and 9.4 Å (Table S2), smaller than the reported experimental value ^{14, 15, 17, 33}. We also studied unform H-termination and ternary mixed termination (O/F/H) and found that the *d*-spacings of these structures are significantly smaller (Table S2) relative to the reported experimental values. In addition, except for the lower H-ratio surfaces that exhibit *d*-spacing and XRD pattern close to the experimental observations (Table S2 & Figure S4), the XRD pattern of ternary mixed termination multilayer (O/F/H) shows a (002) peak located around 11° and is obviously deviated from experimental observation. Thus, this suggests that the formation of uniform terminated Ti₃C₂ and high H-ratio in ternary mixed terminated Ti₃C₂T_x surfaces upon HF etching is shown to be unlikely. In addition, such small *d*-spacing is not favorable for hydrogen diffusion into and subsequent hydrogen storage in the interlayers. Note that the experimentally measured *d*-spacing varied according to several factors, such as the type of etchant (*e.g.*, HF, bifluoride-etchant), acid concentration, and the humidity of the sample (dry or wet). In this study, we only considered experimental synthesized Ti₃C₂T_x etched with HF with O/OH/F as the surface termination group due to the formation of byproducts upon etching.

It is worth mentioning that, despite being energetically less favorable compared to the Poctahedral Ti₃C₂F₂, the P-trigonal Ti₃C₂F₂ with a *d*-spacing of 9.6 Å still exhibited a simulated XRD pattern resembling the features of XRD pattern of the simulated P-octahedral and experimental measurement (Figure S3). In addition, as found in our simulated XRD, the variation of relative intensity in the range of 35-48° is likely to be attributed to the distinct distribution of the surface terminating group. However, detailed insight into such information is generally difficult to provide by experimental XRD characterization. Due to these ambiguities, XRD characterization should be supported by other advanced experimental characterization techniques (*e.g.* XANES, Raman, etc.) and should not be the sole method for the experimental characterization of Ti₃C₂T_x. On the other hand, from the theoretical model point of view, the construction of multilayer Ti₃C₂T_x should be carefully carried out if the experimental *d*-spacing in XRD is the only consideration in the model construction. Thus, with the supports of DFT calculations, this will avoid creating less-stable structures or highly idealized model that would otherwise compromise the reliability of Ti₃C₂T_x models.

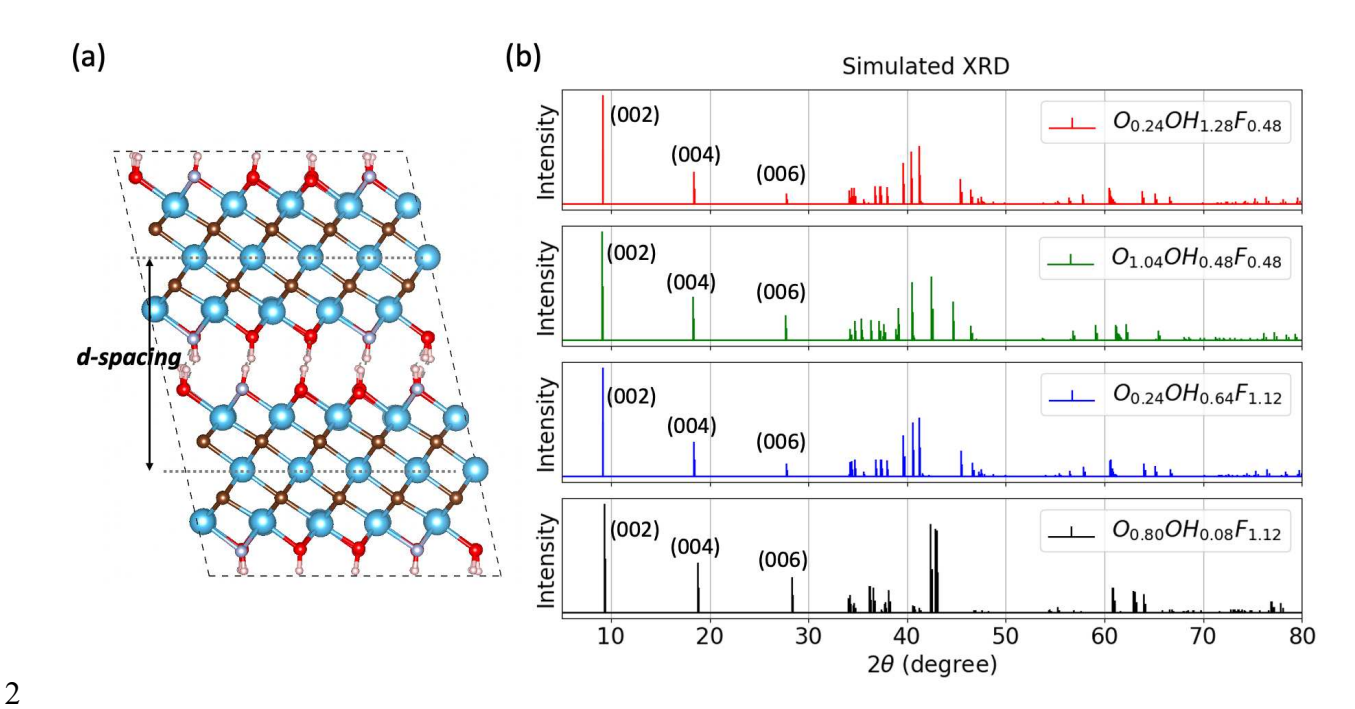


Figure 2. (a) Side view of the ternary mixed O/OH/F-terminated multilayer bulk structure of $Ti_3C_2T_x$ and (b) From the top to the bottom, the simulated XRD of $Ti_3C_2T_x$ with different stoichiometry etched with 5, and 48 wt. % HF.

Figure 3 shows the distribution of d-spacing and the interlayer spacing of $Ti_3C_2T_x$ multilayer structures with different stoichiometry. To better understand the effect of surface termination on the separation between the multilayer, here we define the interlayer separation as the distance between the adjacent planes of the terminating O/F groups in $Ti_3C_2T_x$ multilayer structures. The calculated interlayer separation is 2.43 ± 0.07 Å and is a reasonable range for the diffusion and intercalation of atoms/molecules. Note that, for the 5 wt.% HF etched $Ti_3C_2T_x$ (with a F stoichiometry, r = 0.48), a smaller separation was observed for the surface with a relatively higher OH ratio ($Ti_3C_2O_{0.24}OH_{1.12}F_{0.48}$ and $Ti_3C_2O_{0.48}OH_{1.04}F_{0.48}$). From our finding, this could be due to the enhanced hydrogen bonding between the interlayer surfaces with the increased OH ratio. When the HF concentration is increased (higher F ratio), surface with higher OH ratio would exhibit a slightly smaller separation, but such difference became subtle due to the increased F termination on the surface with an increased repulsion.

Marguis et al. 19 observed a similar difference in the interlayer separation between the uniform F/O terminated and the uniform/binary mixed OH terminated bilayer Ti₂CT_x structure, where F/O terminated bilayer structures demonstrated a larger separation compared to the uniform/binary mixed OH terminated bilayer structure. They suggested that the separation is affected by both the electrostatic repulsion and attraction between different terminating species. In this study, we found a semi-empirical relationship between the O/OH/F ratio and the interlayer separation (see equation in SI and Figure S5), suggesting that the interlayer separation can be described as an empirical function of the terminating group stoichiometry. Interestingly, for each HF concentration, an overestimation in empirical function prediction of the interlayer spacing when the surface transitions towards a higher ratio of OH termination, again, implying that the subtle interlayer interaction (e.g. hydrogen bonding) is important determining the structural properties of the $Ti_3C_2T_x$ multilayer structure. From the optimized structures, we found that the bond distances between the hydrogen of the hydroxyl groups and the F/O termination groups from the adjacent layers are in the range of 1.5-2.1 Å, suggesting the formation of hydrogen bonds between these atoms might contribute to the interlayer binding that affect the d-spacing of multilayer structures. In the following section (Section 3.3), we explore the nature of the interlayer interaction by inspecting the adhesion energy.

1 2

3

4

5

6

7

8

9

10

11

12

13

14

15

16

17

18 19

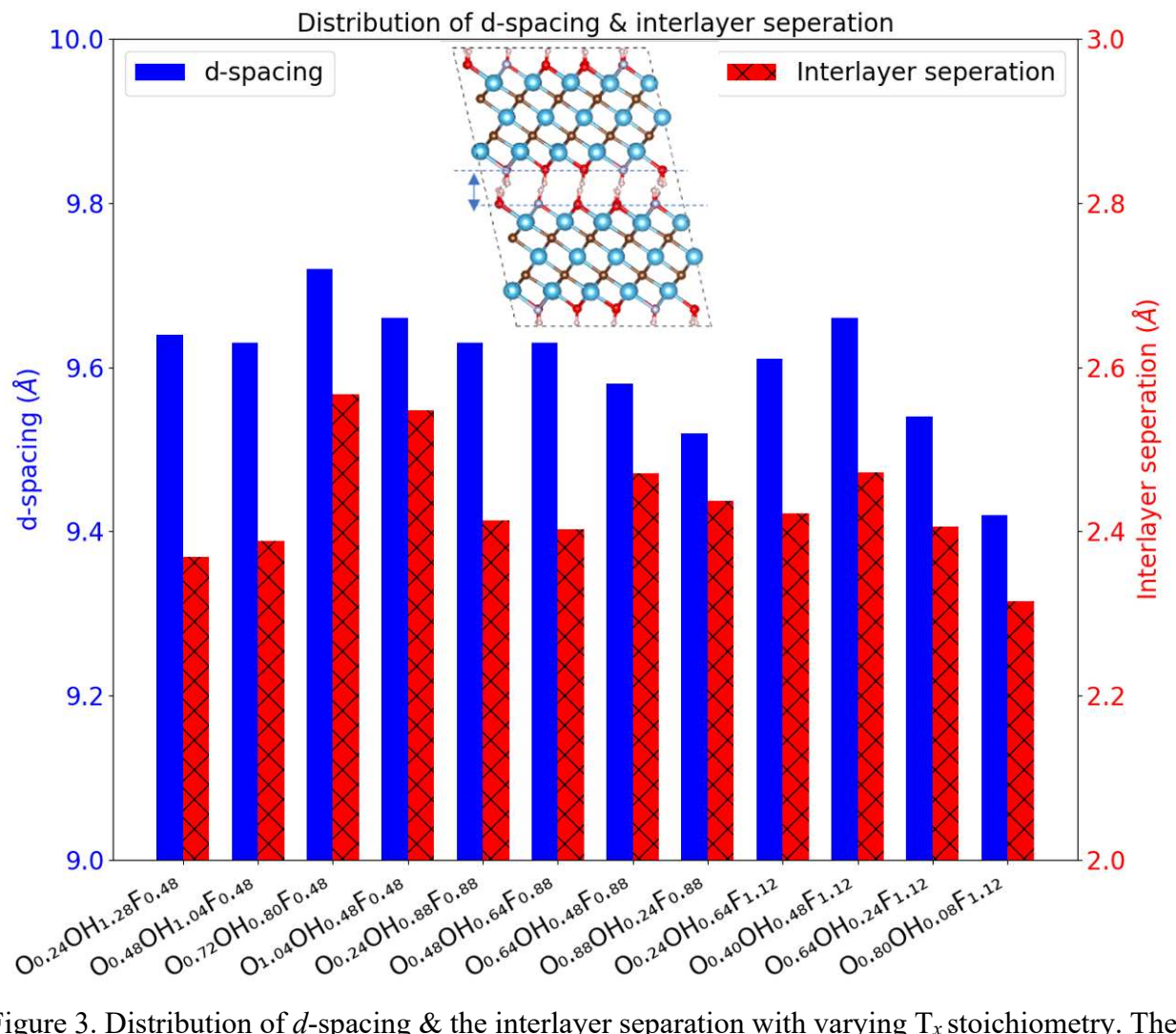


Figure 3. Distribution of *d*-spacing & the interlayer separation with varying T_x stoichiometry. The inset shows the interlayer separation defined in this study. From the left to the right, the $Ti_3C_2T_x$ with different T_x stoichiometry is found by etching with 5, 10, and 48 wt. % HF.

3.3 Adhesion energy

To study the energy required to separate the $Ti_3C_2T_x$ from the multilayer bulk structure, we calculated the adhesion energy, E_{adh} as ¹⁹:

$$E_{adh} = \frac{(2E_{monolayer} - E_{bilayer})}{2A}$$
 (1)

where $E_{bilayer}$, and $E_{monolayer}$ are respectively the total energy of the bilayer and the monolayer considered in $Ti_3C_2T_x$ bulk multilayer structures, and A is the contact area. While d-spacing is a statistically averaged value including the thickness of the $Ti_3C_2T_x$ layers, the interlayer separation is more relevant to the theoretical study of the intercalation of hydrogen or any atoms or molecules and more importantly, directly affects the interlayer interaction. We have performed an analysis and found a subtle relationship between the interlayer separation and the interfacial adhesion energy in the $Ti_3C_2T_x$ multilayers that affected by T_x stoichiometry and HF etching. Figure 4 shows the correlation between the interlayer separation and the adhesion energy distribution of the multilayer Ti₃C₂T_x bulk with different stoichiometry. It is shown that using weak acid (5 wt. % HF) etched Ti₃C₂T_x (i.e. large O:F ratio) in general produced multilayer structures exhibiting stronger adhesion energy compared to that of strong acid (48 wt. % HF) etched Ti₃C₂T_x (i.e. small O:F ratio). The average adhesion energies of the 5 wt.% HF etched multilayer $Ti_3C_2T_x(0.94 \pm 0.11$ J/m^2) are about 0.30 J/m^2 stronger than that of the 48 wt.% HF etched multilayer $Ti_3C_2T_x$ (0.65 \pm 0.04 J/m²). Our calculation shows that an increase in the interlayer separation would lead to a weaker adhesion energy. Intuitively, a larger separation would result in a weaker interaction between the adjacent layers, thus, inducing a smaller adhesion energy. Intriguingly, this trend does not hold for structures etched with 48 wt.% HF which has largest F content. When the interlayer separation decreases, we observe a decrease in the adhesion energy instead of an enhanced adhesion energy as observed for the case of 5 wt.% and 10 wt. % especially for OH-poor in T_x stoichiometry. When the surface becomes F dominant (etched with 48 wt.% HF) with lesser OH content, the electrostatic repulsion between adjacent F terminal groups becomes increasingly dominant, especially when the interlayer separation is smaller. This, in turn, decreases the interlayer interaction and the adhesion energy.

1 2

3

4

5

6

7

8

9

10

11

12

13

14

15

16

17

18

19

20

21

22

23

24

25

26

27

28

29

30

31

For uniform terminated multilayer structures, $Ti_3C_2F_2$ demonstrated the weakest adhesion energy (0.49 J/m²) while $Ti_3C_2O_2$ and $Ti_3C_2OH_2$ showed slightly stronger interactions (0.75 and 0.83 J/m²). The lowest adhesion energy is due to the strong repulsion between the interlayer F adatoms ¹⁹ and the enhanced interlayer interaction between $Ti_3C_2OH_2$ is due to the substantial hydrogen bonds in between the adjacent hydroxyl group. The observation in the uniform terminated multilayer structures provides a simple explanation for the observed trend in Figure 4. With a simple fitting formula based on the adhesion energies of uniform termination multilayer $Ti_3C_2T_x$ and the mixed T_x stoichiometry, we derived a semi-empirical formula to fit the calculated

adhesion energy (see equation in SI and Figure S6). We notice that the fitting formula is generally accurate, however tends to underestimate the adhesion energy of the surface etched with the least acidic HF, *i.e*, surface with a large OH ratio. Note that the fitting formula did not include additional energy interaction (*e.g.* hydrogen bond) among the $Ti_3C_2T_x$ layers. Such a trend can be explained by the interlayer bond strength attributed to different terminal groups (O/OH/F/H) which will be discussed in the following section (Section 3.4).

1 2

3

4

5

6

7

8

9

10

11

12

13

14

15

16

17

18

19

20

21

22

23

24

25

26

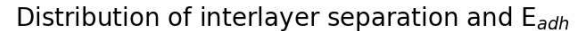
27

28

29

30

In a recent adhesion and friction study of MXene, Li et al. 34 performed the first experimental research on MXene interlayer interactions using atomic force microscopy (AFM) probe coated with $Ti_3C_2T_x$ and found a strong adhesion energy between the $Ti_3C_2T_x$ interface with a measured adhesion energy of ~1.23 J/m². In a later study conducted by Luo et al. ³⁵ employing a slightly different AFM probe geometry, they measured the adhesion energy to be 0.404 ± 0.012 J/m². The discrepancy could be attributed to the distinct probe coating methods and the probe geometries employed in the studies ³⁵. Nevertheless, our calculated average adhesion energy, 0.77 ± 0.15 J/m² is consistent within the range of experimentally measured value ($\sim 0.39 - 1.23$ J/m²) ³⁴, ³⁵ and slightly larger than other 2D materials such as graphene (0.328 \pm 0.028 J/m²), hBN (0.326 \pm 0.026 J/m²) and MoS₂ (0.482 \pm 0.032 J/m²) ³⁶. Complementary to ternary mixed O/OH/F terminated structures, we also calculated the adhesive energies of several quaternary mixed F/O/OH/H multilayer Ti₃C₂T_x structures (Table S3) where the adhesion energies are comparable to that of the ternary mixed O/OH/F mixed terminated multilayer Ti₃C₂T_x structures. If, however, when considering the ternary mixed O/F/H terminated surface (i.e. O_{0.24}F_{0.48}H_{1.28} in Table S3), a significantly larger adhesion energy is obtained (1.1 J/m²) compared to the calculated average energy value of 0.77 ± 0.15 J/m². Note that, a uniform H-terminated Ti₃C₂ multilayer also demonstrated a profoundly large (3.4 J/m²) in adhesion energy. Judging from the comparable Ti-H bond length (~1.9 Å) and the strong adhesion energy, we speculate that such interaction is similar to the Ti-H bonding (1.21 eV) found in titanium hydride TiH₂ bulk. Hence, we calculated and compared the COHP (see Section 3.4 for details) of these two structures and confirmed our speculation. Thus, in addition to the discrepancy found in d-spacing (Table S2) and XRD analysis, from the calculated adhesion energy, we can safety exclude the possibility of the formation of Ti₃C₂H₂ and high H-ratio in mixed terminated multilayer Ti₃C₂T_x structures upon HF etching.



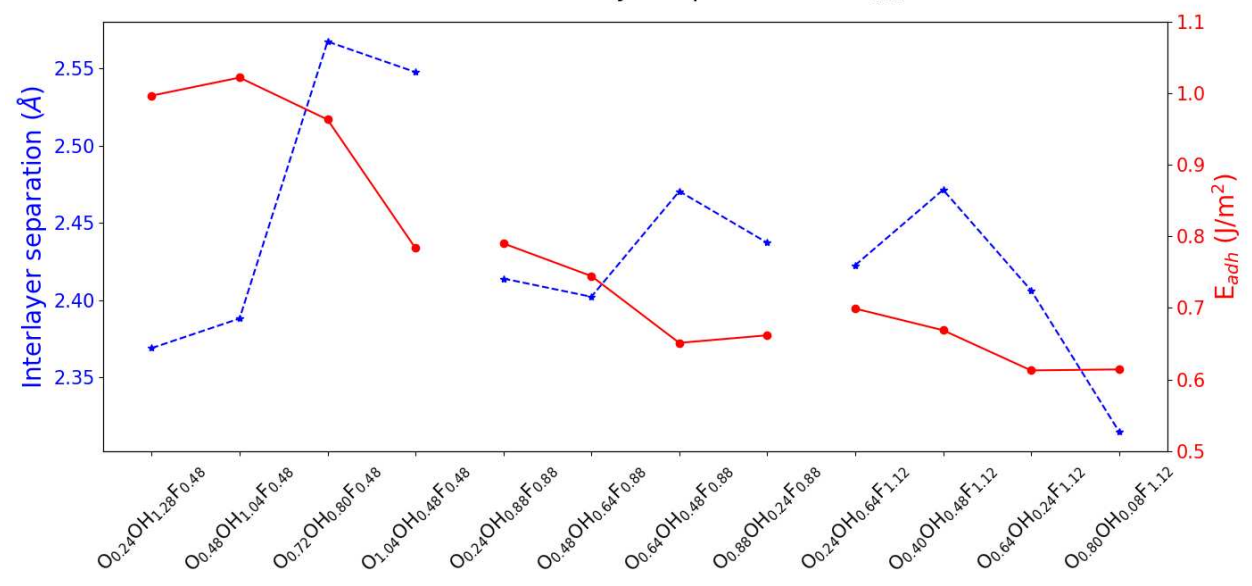


Figure 4. Distribution of interlayer separation and adhesion energy with varying T_x stoichiometry. From the left to the right, the $Ti_3C_2T_x$ with different T_x stoichiometry is found by etching with 5, 10, and 48 wt. % HF.

3.4 Electronic properties and COHP

To study the electronic properties and the bonding feature of multilayer $Ti_3C_2T_x$, we calculated the band structure, density of states, and the -COHP around the Fermi level (Figure 5). The uniform terminated (Figure S7) and mixed terminated multilayer $Ti_3C_2T_x$ exhibit metallic characteristics, similar to those of monolayer $Ti_3C_2T_x$ (Figure S8)^{18, 37}. In general, the structures with different T_x stoichiometry all showed similar metallic-like in electronic structures and properties. For the conciseness and clarity of discussion, we only included one of the $Ti_3C_2T_x$ multilayer structures ($T_x = O_{0.24}OH_{1.28}F_{0.48}$) in Figure 5. The inset in the eDOS in Figure 5 shows the presence of H, F, and O finite electronic states near the Fermi level. To further study the bonding characteristics of these elemental orbitals, we take the average -COHP of the adjacent layer of H-O and H-F pairs and plotted the -COHP. It is interesting to see that these atomic pairs show bonding characteristics around the Fermi level, suggesting hydrogen bonding interaction of H-O and H-F between the multilayers.

Figure 6 (a) and (b) show the charge density difference of multilayer $Ti_3C_2T_x$. There is a significant charge accumulation between the O-H and F-H pair from the adjacent layer, suggesting substantial interlayer interaction, such as hydrogen bonds are possibly formed between these

functional groups. As a result, larger adhesion energy is required to separate the layers (*i.e.* $T_x = O_{0.24}OH_{1.28}F_{0.48}$ in Figure 4) apart. Since, intuitively, a lower HF concentration would result in a lower probability for F to terminate on the surface, in turn, increase the relative OH ratio on the surface, we would see a large amount of hydrogen bond formed in between the adjacent layer which is reflected by the increased adhesion energy as shown in Figure 4. In addition to the hydrogen bonds formed between the O-H pair, it is also possible for the F-H pair between the adjacent layer to form hydrogen bonds with comparable strength as shown in the charge density difference plot (Figure 6 (a) and (b)). Hence for T_x with large O:F ratio (*e.g.* $O_{0.24}OH_{1.28}F_{0.48}$), the OH-terminating group is responsible for the overall increase of adhesion energy as a large surface OH ratio maximizes the possibility of hydrogen bond formation.

1 2

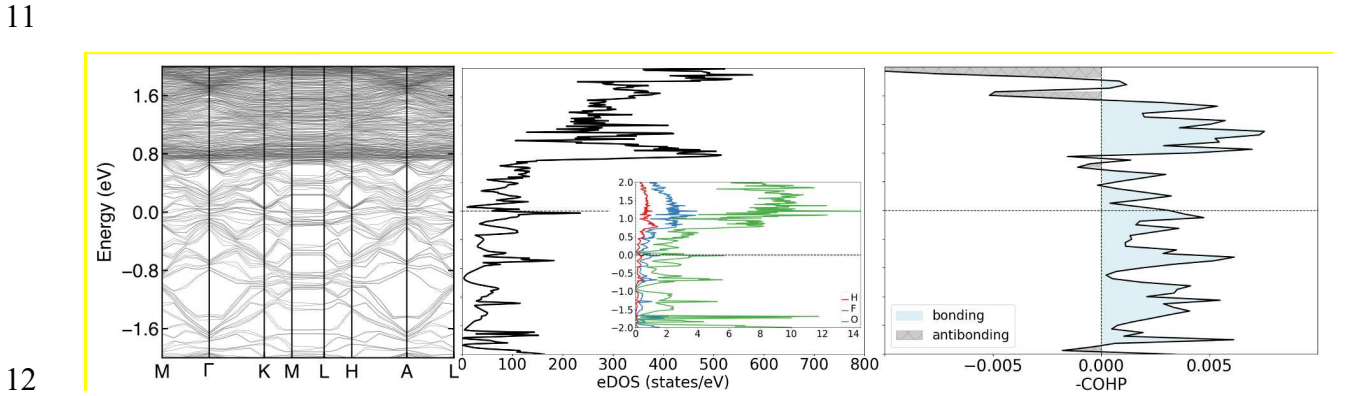


Figure 5. Electronic band structure (left), electronic density of states (center) and -pCOHP (right) of multilayer $Ti_3C_2T_x$. ($T_x = O_{0.24}OH_{1.28}F_{0.48}$). The multilayer $Ti_3C_2T_x$ shows metallic features. The adjacent layers of H-O and H-F pairs are the atomic pairs selected for the -pCOHP plot.

To quantitatively study the bond strength, we further calculated the COHP between different atomic pairs and summarized the integrated COHP in Figure 6 (c). In analogy to the eDOS where the energy integration of eDOS up to E_F results in the number of valence electrons, the energy integration of all COHP for a pair of atoms up to E_F (ICOHP) yields the bond strength $^{27-30}$. Intuitively, the bond strength is a function of the atom pair distances which decreases with increased pair distance. In addition, in Figure 6 (c), we found that the H-F and H-O pair from different layers both demonstrated a bond strength of 0.93-1.2 eV, which is comparable to a typical hydrogen bond strength 38 , consistent with the charge density difference observed in Figure 6 (a), (b) and further confirming the significant formation of hydrogen bonds between these terminating atoms. Thus, in theory, a strong acid etched $T_{13}C_2T_x$ might be easier to exfoliate owing to the

slightly weaker adhesion energy (Figure 4) because of fewer hydrogen bonding present in between the adjacent layers. In contrast, the weaker adhesion energies of multilayer $Ti_3C_2T_x$ etched with stronger HF are reflected in the relatively smaller bond strengths of F-F, O-O and F-O pairs (~0.01-0.20 eV) as shown in Figure 6 (c). Interestingly, for the 5 wt.% HF etched $Ti_3C_2T_x$ (with a F stoichiometry, r = 0.48, Figure 3), a slightly larger separation was observed for the surface with a relatively higher O ratio ($Ti_3C_2O_{0.72}OH_{0.80}F_{0.48}$ and $Ti_3C_2O_{1.04}OH_{0.48}F_{0.48}$ in Figure 3), is possibly due to more F-O/O-O pairs present in the interlayer surfaces. Thus, this suggests that for the hydrogen stored or diffused into interlayer of $Ti_3C_2T_x$, the subtle influence of hydrogen bonds and the interactions among the surface O/OH/F termination groups between the adjacent layers in $Ti_3C_2T_x$ multilayers cannot be ignored.

1 2

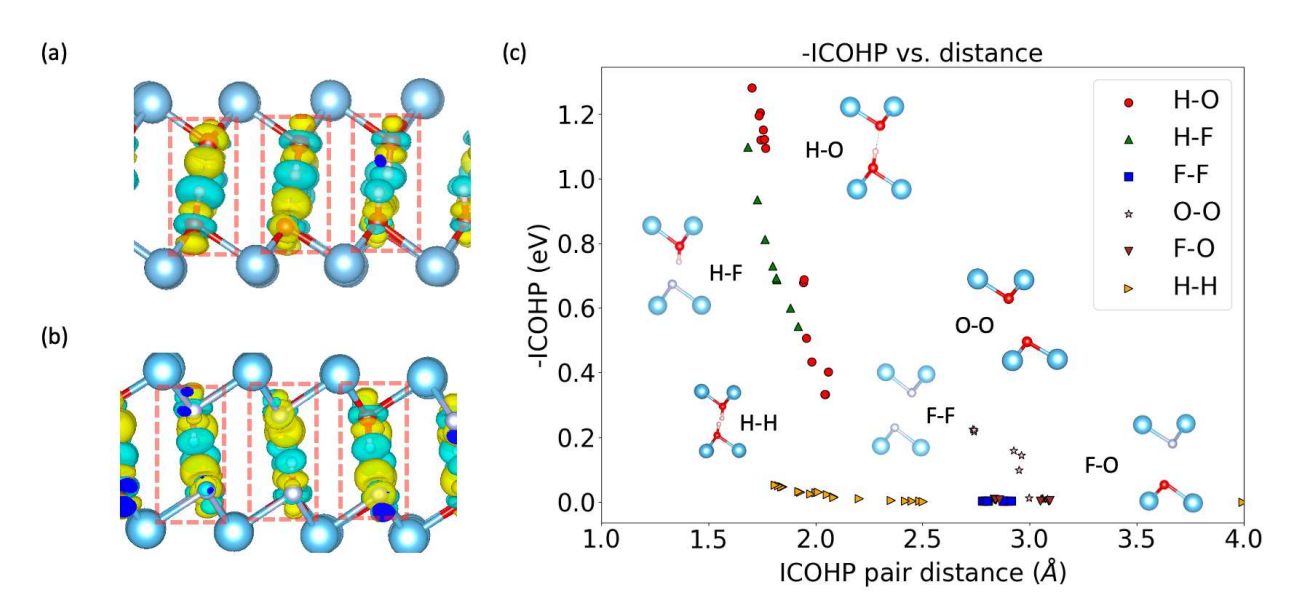


Figure 6. The charge density difference interlayer of multilayer $Ti_3C_2T_x$ with (a) $T_x = O_{0.24}OH_{1.28}F_{0.48}$ (etched with 5 wt. % HF) and (b) $T_x = O_{0.24}OH_{0.64}F_{1.12}$ (etched with 48 wt. % HF) with isovalue 0.002 e/Å³. Yellow and blue regions highlighted in the dashed red box represent charge accumulation and depletion respectively. (c) The -ICOHP distribution as a function of pair distance. Inset shows the atomic pairs considered for the ICOHP calculation. Color code: Blue-Ti, Red-O, Pink-H, Purple-F.

3.5 Effect of water and hydrogen on the structural properties

2 3 4

5

6

7

8

9

10

11

12

13

14

15

16

17

18

19

20

21

22

23

24

25

26

27

28

29

1

It is known that the humidity of the $Ti_3C_2T_x$ sample can affect the XRD spectra ^{13, 14}. To investigate the effect of water molecules on the d-spacing, we constructed a wet multilayer $Ti_3C_2T_x$ model with H₂O molecules intercalated in between the interlayer spacing. Here, we considered the stoichiometry $T_x = O_{0.24}OH_{1.28}F_{0.48}$ intercalated with 1 (Ti₃C₂T_x·H₂O) and 2 layers of water $(T_{i3}C_2T_x\cdot 2H_2O)$. Figure 7 (a), and (b) show the optimized structure of the wet multilayer $T_{i3}C_2T_x$ with different amounts of H₂O and the high H-ratio in ternary mixed O/F/H Ti₃C₂T_x with the focus on interlayer separation. From DFT results, the calculated d-spacing is proportional to the amount of water molecules present in the interlayer where the d-spacing increases from 12.5 ($Ti_3C_2T_x \cdot H_2O$) to 14.6 Å (Ti₃C₂T_x·2H₂O), and is consistent with reported theoretical and experimentally observed values $^{13, 14, 39}$ within the range of ~12.5-14.8 Å. The predicted d-spacing suggested that the intercalated H₂O behaved in a nanoconfined-like water structure as opposed to that of bulk water molecules. In a recent study by Wu et al. ³⁹ on the water/Ti₃C₂O₂ interfacial interaction, they found that water would attack the basal plane of the uniformly terminated MXene surface as initiated by the water adsorption, affecting the overall structural stability of Ti₃C₂O₂. In addition, increasing surface OH termination on Ti₃C₂O₂ would render the surface less susceptible to water attack. In our DFT study, we did not observe strong water adsorption but instead found spontaneous deprotonation of the water molecules and the subsequent formation of OH bonds on the readily Ofunctionalized surface. A slight increase in the deprotonation rate was observed (from 1% to 3%) when 2 layers of water molecules were present compared to that of single-layer water in Ti₃C₂T_x multilayers. Overall, the structural integrity was preserved with even two layers of H₂O. This suggests that ternary O/OH/F mixed terminated Ti₃C₂T_x surfaces exhibit higher resistance against the water attack, relative to the reported Ti₃C₂O₂ ³⁹. In terms of the bonding properties, our COHP (Table S4) and charge density difference calculation (Figure 8) also show that strong hydrogen bonds were found between the terminated hydroxyl group and the O from the water, and the hydroxyl group from the water with the terminated O and F adatom, similar to the dry structures aforementioned (Section 3.4).

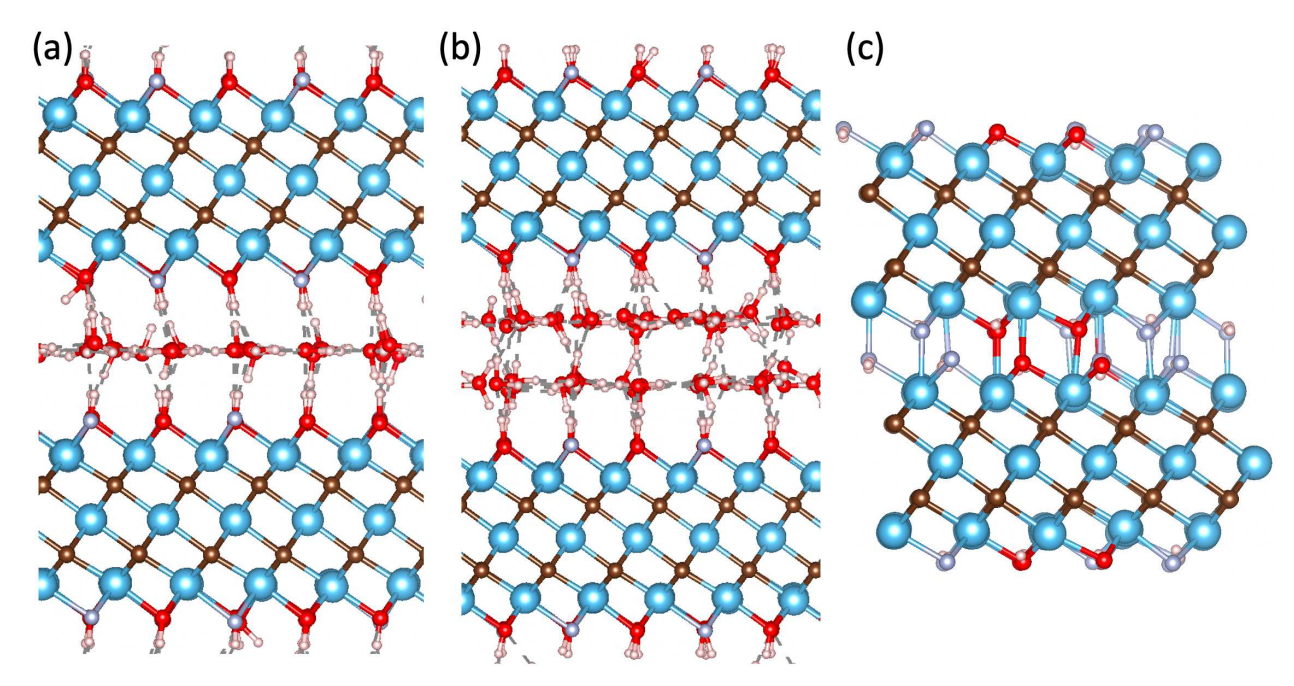


Figure 7. Side view of the optimized multilayer $Ti_3C_2T_x$ bulk intercalated with H_2O molecules (a) $Ti_3C_2T_xO_{0.24}OH_{1.28}F_{0.48}\cdot H_2O$, (b) $Ti_3C_2T_xO_{0.24}OH_{1.28}F_{0.48}\cdot 2H_2O$ and (c) $Ti_3C_2T_xO_{0.24}F_{0.48}H_{1.28}$.

1

3

4

5

6

7

8

9

10

1112

13

14

15

16

17

18

19

20

As opposed to the increase of the d-spacing with the intercalated H_2O , a significant shrinkage of the d-spacing (Table S2) was observed when the multilayer Ti₃C₂T_x surface was terminated with a high ratio of hydrogen adatom. Here, we consider a uniform H-terminated surface and a ternary O/F/H-terminated surface (i.e. $T_x = O_{0.24}F_{0.48}H_{1.28}$) to study the bond strength employing COHP. Both the bond length and the COHP calculation show that the interaction between the Ti-H pair from the adjacent layer is comparable to the bulk titanium hydride (Table S4), TiH₂, which explains the significantly smaller d-spacing (Table S2) due to the strong Ti-H interaction, and as a result, attracting the adjacent layers close to each other with larger adhesion energy ($E_{adh} = 1.09 \text{ J/m}^2$ in Table S3). Interestingly, in addition to the Ti-H bond, we also observed strong Ti-O and Ti-F bonding in the ternary O/F/H-terminated multilayer $Ti_3C_2T_x$ ($T_x =$ O_{0.24}F_{0.48}H_{1.28}) which is comparable to the bulk titanium fluoride, TiF₃, and titanium oxide, TiO₂ respectively (Table S4). These interactions are responsible for the larger adhesion energy and the significantly smaller d-spacing compared to the uniform or ternary F-/O-/OH-terminated Ti₃C₂T_x. Note that, such small d-spacing (\sim 7.4-7.9 Å) was not found in the experimental synthesized multilayer Ti₃C₂T_x. Thus, from our DFT calculation, it can be concluded that the experimentally synthesized multilayer $Ti_3C_2T_x$ would have minimal H-termination.

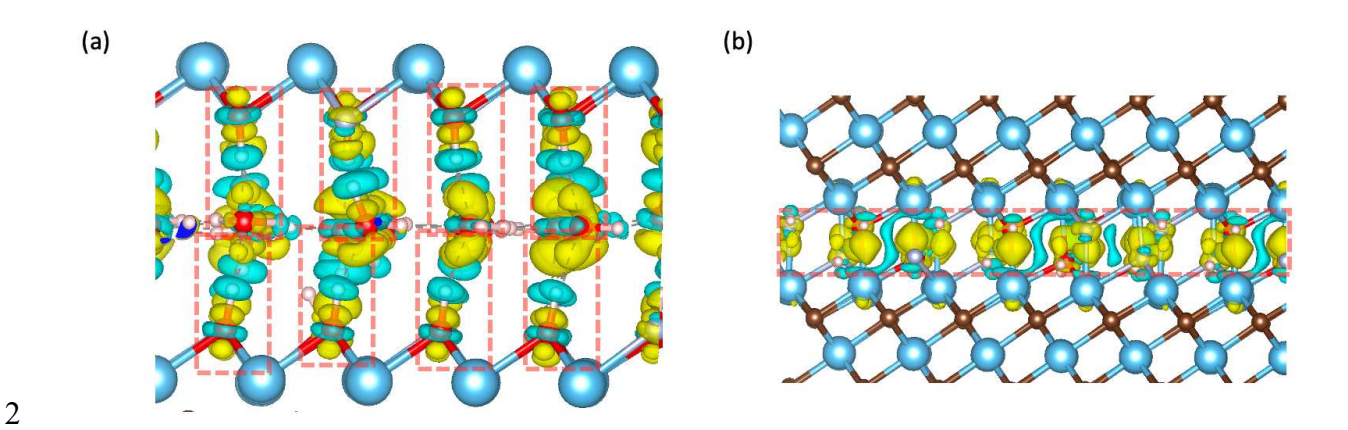


Figure 8. Charge density difference of (a) $Ti_3C_2T_x \cdot H_2O$ and (b) $Ti_3C_2T_xO_{0.24}F_{0.48}H_{1.28}$. Yellow and blue regions highlighted in the dashed red box represent charge accumulation and depletion respectively with isovalue of 0.004 e/Å³ and color code: Blue-Ti, Red-O, Pink-H, Purple-H.

4. CONCLUSION

We have carried out a systematic study on the structural and electronic properties of the multilayer $Ti_3C_2T_x$ MXene considering various T_x stoichiometry that representing different HF concentrations (5, 10 and 48 wt. % HF) as the etchant in synthesis. The calculated average d-spacing (9.60 \pm 0.07 Å) and the simulated XRD spectra are consistent with the reported experimental findings^{14, 15, 17, 33}. The calculated d-spacing and powder XRD spectra analysis suggested that the formation of uniform termination, particularly H-termination is unlikely due to a notably smaller d-spacing compared to experimental measurements. Even with a mixed termination, a high ratio of surface H-termination would result in a significant shrinkage of the d-spacing because of the formation of strong ionic Ti-H bonds between the interlayers. Thus, for the uniform H-termination and high H-ratio in mixed terminated $Ti_3C_2T_x$ multilayers, this suggests that a significant decrease in d-spacing is not favorable for the diffusion of atoms or molecules into the interlayers.

From our finding, the interlayer separation is essentially governed by the surface termination group, especially when OH species is dominant on the surface. In terms of adhesion energy, the calculated adhesion energy shows that multilayer $Ti_3C_2T_x$ etched with weak acidic HF demonstrated an enhanced interlayer interaction compared to that of strong acidic HF, due to the

increased OH and decreased F ratio on the surface. The average adhesion exergy of O/OH/F-ternary mixed $Ti_3C_2T_x$ multilayers is predicted to be 0.77 ± 0.15 J/m² and is comparable to the reported experimental measurements ($\sim 0.39 - 1.23$ J/m²) ^{34, 35}. Similar to the *d*-spacing, the calculated adhesion energy of $Ti_3C_2H_2$ and dominantly high H-content in ternary or quaternary mixed termination of $Ti_3C_2T_x$ multilayers is inconsistent with experimental observations, which further confirmed that the presence of uniform H-termination of Ti_3C_2 or dominantly high H-content in ternary or quaternary mixed termination of $Ti_3C_2T_x$ multilayers is unlikely.

In the current study, we found that the electronic density of states of all multilayer $Ti_3C_2T_x$ are similar to those of metallic Ti₃C₂T_x monolayers [Ref18]. The uniform terminated and mixed terminated multilayer Ti₃C₂T_x exhibit metallic characteristics, similar to those of monolayer $Ti_3C_2T_x$ and which predicted in Ref[18]. Besides, the COHP calculation proved that the increased interaction between the weak HF (5 wt. % HF) etched Ti₃C₂T_x multilayer is attributed to the enhanced hydrogen bonding nature between the H atoms of the hydroxyl group and the adjacent F/O termination group. Thus, theoretically, using a stronger HF as an etchant would produce multilayer Ti₃C₂T_x with a lesser OH terminating group, resulting in the minimization of the hydrogen bonding between the interlayers and easier to exfoliate. We have also studied the wet multilayer $Ti_3C_2T_x$ by intercalating up to two layers of water between the interlayer and found that the *d*-spacing is also consistent with theoretical and experimental values $(12.5 - 14.6 \text{ Å})^{13, 14, 39}$. Interestingly, according to DFT calculations, unlike bulk water molecules, the nanoconfined water molecules are restricted on a 2D plane, which could provide an interesting avenue to explore in future novel materials applications. Meanwhile, although current experimental studies showed that the Ti₃C₂T_x surfaces are mixed terminated, there have been efforts to produce MXenes with uniform termination ⁴⁰. We believe that our current findings offer fundamental insight into this endeavor in addition to providing a design pathway for the synthesis of monolayer Ti₃C₂T_x. From the theoretical simulation point of view, the multilayer $Ti_3C_2T_x$ structure motifs constructed in this study have been proven to be a valid model and could serve as a more complicated yet realistic next-generation model for future simulation of multilayer $Ti_3C_2T_x$ MXene in various applications.

CONFLICTS OF INTEREST

1 2

3

4

5

6

7

8

9

10

11

12

13

14

15

16

17

18

19

20

21

22

23

24

25

26

27

28

29

30

31 32 There are no conflicts of interest to declare.

DATA AVAILABILITY

1 2

3 The data supporting this article have been included as part of the Supplementary Information.

4 5

ACKNOWLEDGEMENT

6

- 7 The contribution of computing resources through NSF-MRI: NSF OAC-2117956 is acknowledged.
- 8 The authors acknowledge the support of the U.S. Department of Energy, Office of Science, Office
- 9 of Basic Energy Sciences, Division of Materials Sciences and Engineering. The authors also
- 10 acknowledge the partial support of the U.S. Research Corporation for Science Advancement
- 11 (RCSA) through the Cottrell Scholar Award (Award No. 26829). The authors would like to extend
- their gratitude to Prof. Yury Gogotsi, Dr. Megan Hoover, and Dr. Patrick Ward for their valuable
- and insightful discussion and comments during the preparation of this paper.

14 15

REFERENCES

16 17

- 18 1. M. Naguib, M. Kurtoglu, V. Presser, J. Lu, J. Niu, M. Heon, L. Hultman, Y. Gogotsi and M. W. Barsoum, *Advanced Materials*, 2011, **23**, 4248-4253.
- 20 2. Y. Gogotsi and B. Anasori, ACS Nano, 2019, 13, 8491-8494.
- 21 3. E. Lee and D.-J. Kim, *Journal of The Electrochemical Society*, 2020, **167**, 037515.
- U. Yorulmaz, İ. Demiroğlu, D. Çakir, O. Gülseren and C. Sevik, *Journal of Physics: Energy*, 2020, 2, 032006.
- 5. Y. Xie, M. Naguib, V. N. Mochalin, M. W. Barsoum, Y. Gogotsi, X. Yu, K.-W. Nam, X.-Q. Yang, A. I. Kolesnikov and P. R. C. Kent, *Journal of the American Chemical*
- 26 Society, 2014, **136**, 6385-6394.
- Q. Hu, D. Sun, Q. Wu, H. Wang, L. Wang, B. Liu, A. Zhou and J. He, *The Journal of Physical Chemistry A*, 2013, 117, 14253-14260.
- 29 7. Y. Z. Chu and K. C. Lau, *International Journal of Hydrogen Energy*, 2024, **57**, 1144-30 1151.
- 31 8. S. Liu, J. Liu, X. Liu, J. Shang, L. Xu, R. Yu and J. Shui, *Nature Nanotechnology*, 2021, **16**, 331-336.
- S. Ghotia, A. Kumar, V. Sudarsan, N. Dwivedi, S. Singh and P. Kumar, *International Journal of Hydrogen Energy*, 2023, DOI: https://doi.org/10.1016/j.ijhydene.2023.05.145.
- 35 10. T. Thomas, S. Bontha, A. Bishnoi and P. Sharma, *Journal of Energy Storage*, 2024, **88**, 111493.
- 37 11. S. Patchkovskii, J. S. Tse, S. N. Yurchenko, L. Zhechkov, T. Heine, G. Seifert and J. L.
- Dye, *Proceedings of the National Academy of Sciences of the United States of America*, 2005, **102**, 10439-10444.
- 40 12. L. Yang, X. Li, G. Zhang, P. Cui, X. Wang, X. Jiang, J. Zhao, Y. Luo and J. Jiang, *Nature Communications*, 2017, **8**, 16049.

- 1 13. Y. Ying, Y. Liu, X. Wang, Y. Mao, W. Cao, P. Hu and X. Peng, *ACS Applied Materials & Interfaces*, 2015, 7, 1795-1803.
- 3 14. H.-W. Wang, M. Naguib, K. Page, D. J. Wesolowski and Y. Gogotsi, *Chemistry of Materials*, 2016, **28**, 349-359.
- 5 15. S. Wang, Y. Liu, Y. Liu and W. Hu, Chemical Engineering Journal, 2023, 452, 139512.
- 6 16. F. Kong, X. He, Q. Liu, X. Qi, Y. Zheng, R. Wang and Y. Bai, *Electrochimica Acta*, 2018, **265**, 140-150.
- 8 17. X. Wang, X. Shen, Y. Gao, Z. Wang, R. Yu and L. Chen, *Journal of the American Chemical Society*, 2015, **137**, 2715-2721.
- 10 18. Y. Z. Chu, M. Hoover, P. Ward and K. C. Lau, iScience, 2023.
- 11 19. E. Marquis, M. Cutini, B. Anasori, A. Rosenkranz and M. C. Righi, *ACS Applied Nano Materials*, 2022, **5**, 10516-10527.
- 13 20. G. Kresse and J. Furthmüller, Computational Materials Science, 1996, 6, 15-50.
- 14 21. G. Kresse and J. Furthmüller, *Physical Review B*, 1996, **54**, 11169-11186.
- 15 22. J. P. Perdew, K. Burke and M. Ernzerhof, *Physical Review Letters*, 1996, 77, 3865-3868.
- 16 23. S. Grimme, Journal of Computational Chemistry, 2006, 27, 1787-1799.
- 17 24. A. S. Tygesen, M. Pandey, T. Vegge, K. S. Thygesen and J. M. García-Lastra, *The Journal of Physical Chemistry C*, 2019, **123**, 4064-4071.
- 19 25. J. Hadler-Jacobsen, F. H. Fagerli, H. Kaland and S. K. Schnell, *ACS Materials Letters*, 20 2021, **3**, 1369-1376.
- 21 26. J. Hadler-Jacobsen and S. K. Schnell, *Advanced Materials Interfaces*, 2022, **9**, 2200014.
- 22 27. R. Nelson, C. Ertural, J. George, V. L. Deringer, G. Hautier and R. Dronskowski, *Journal of Computational Chemistry*, 2020, **41**, 1931-1940.
- 24 28. S. Maintz, V. L. Deringer, A. L. Tchougréeff and R. Dronskowski, *Journal of Computational Chemistry*, 2013, **34**, 2557-2567.
- 29. V. L. Deringer, A. L. Tchougréeff and R. Dronskowski, *The Journal of Physical Chemistry A*, 2011, 115, 5461-5466.
- 28 30. R. Dronskowski and P. E. Bloechl, *The Journal of Physical Chemistry*, 1993, **97**, 8617-8624.
- 30 31. C. F. Bunge, J. A. Barrientos and A. V. Bunge, *Atomic Data and Nuclear Data Tables*, 1993, **53**, 113-162.
- 32 32. K. Momma and F. Izumi, Journal of Applied Crystallography, 2011, 44, 1272-1276.
- 33. M. Alhabeb, K. Maleski, B. Anasori, P. Lelyukh, L. Clark, S. Sin and Y. Gogotsi, 34. *Chemistry of Materials*, 2017, **29**, 7633-7644.
- 35 34. Y. Li, S. Huang, C. Wei, D. Zhou, B. Li, C. Wu and V. N. Mochalin, *ACS Applied Materials & Interfaces*, 2021, **13**, 4682-4691.
- 35. S. Luo, T. Alkhidir, S. Mohamed, S. Anwer, B. Li, J. Fu, K. Liao and V. Chan, *Applied Surface Science*, 2023, **609**, 155303.
- 39 36. H. Rokni and W. Lu, *Nature Communications*, 2020, 11, 5607.
- 40 37. K. E. White, Y. Z. Chu, G. Gani, S. Ippolito, K. K. Barr, J. C. Thomas, A. Weber-
- 41 Bargioni, K. C. Lau, Y. Gogotsi and P. S. Weiss, *Matter*, 2024, 7, 2609-2618.
- 42 38. S. Nakamura, Y. Tsuji and K. Yoshizawa, *ACS Omega*, 2020, **5**, 26211-26219.
- 43 39. T. Wu, P. R. C. Kent, Y. Gogotsi and D.-e. Jiang, *Chemistry of Materials*, 2022, **34**, 4975-4982.
- 45 40. V. Natu and M. W. Barsoum, *The Journal of Physical Chemistry C*, 2023, **127**, 20197-20206.